

## **FOCUSING OF ELECTROMAGNETIC WAVE FROM HYPERBOLIC LENS INTO A UNIAXIAL CRYSTAL WITH AN ARBITRARY ORIENTATION OF THE OPTICAL AXIS IN THE PRESENCE OF ABERRATIONS**

**A. Ghaffar and H. Liaquat**

Department of Physics  
University of Agriculture  
Faisalabad, Pakistan

**Q. A. Naqvi**

Department of Electronics  
Quaid-i-Azam University  
Islamabad, Pakistan

**Abstract**—We derive integral representations suitable for studying the focusing of electromagnetic waves through a symmetrically hyperbolic focusing lens into uniaxial crystal in the presence of cylindrical and coma aberrations using Maslov's method. The uniaxial crystal used is the negative crystal  $\text{LiNbO}_3$ . Numerical computations are made to obtain the results for focused fields inside negative uniaxial crystal with several different orientations of the optical axis in the plane of incidence. The effects of aberrations inside uniaxial crystal and isotropic medium are also noted. The results are compared with those obtained by Kirchhoff-Huygens integral and Maslov's method which are in good agreement.

### **1. INTRODUCTION**

Anisotropic uniaxial materials are used in many components such as polarizers, birefringent filters and liquid crystal displays. These media exhibit birefringence. One of the rays, called an ordinary ray, satisfies Snell's law of refraction, and calculations of its propagation are the same as those for an isotropic medium. The second ray is called an

---

*Received 4 July 2010, Accepted 12 August 2010, Scheduled 19 August 2010*  
Corresponding author: A. Ghaffar (chabdulghaffar@yahoo.com).

extraordinary ray, and does not satisfy Snell's law of refraction, and calculations of its propagation are slightly more difficult. The problem of ray tracing in uniaxial crystals has been solved in different forms by several authors during the last decades [1–14].

The analysis of refraction of electromagnetic waves through a symmetrically focusing system into two media becomes very complicated when one or both of the media become uniaxially anisotropic. The complication is called mode coupling. Mode coupling occurs when an incident plane wave (either ordinary or extraordinary) produces both ordinary and extraordinary reflected plane waves and/or produces both ordinary and extraordinary transmitted waves. If we choose special orientations of the optical axis with respect to the interface normal and/or the direction of propagation of the incident plane wave mode coupling can be avoided.

Various kinds of high frequency techniques are used to determine focal or caustic region field under different conditions. Every technique has its own merits and demerits. For example, Huygens Kirchhoff integral and Deby approximation are two high frequency techniques. Former technique is based on low Fresnel approximation whereas later is based on high Fresnel approximation. When we apply these techniques to axially symmetrical three dimensional problems, we must perform a double integration because we cannot use the Fresnel approximation for the kernel. Many investigations on the fields in focal space of reflector and lens antennas into isotropic and uniaxially anisotropic media have been carried out [15–17] using Huygens Kirchhoff integral and Deby approximation.

Geometrical optics approximation for waveform modelling is an attractive in electromagnetics because it provide insight into how a wave front responds to a given structure. In this technique, user has the luxury of being able to monitor a given phase as it steps through the medium. GO is concerned only with the relatively high frequency component of the waveform, provided the ray tube does not vanish. However, there exist regions where ray tube shrinks to zero, called caustics and GO fails there.

A systematic procedure which remedies these defects is Maslov's method. GO field can be formulated in spatial domain, in wave vector domain, or in a combination of the both domains may be termed as phase space. The formulation in wave vector domain is equivalent to the ray description of the Fourier transform of the wave field. This transformation eliminates the occurrences of the ray singularity [18–27].

In present discussion, we have considered a focusing geometry which contains a hyperbolic lens at a certain distance from plane

uniaxial interface. For the special case in which the incident field is a transverse magnetic (TM) plane wave polarized in the  $xz$  plane, which is the plane of incidence, considerable simplifications occur, especially if we also let the optical axis in the crystal to be in the plane of incidence. In this case the refracted field is superposition of ordinary and extraordinary waves behaves as TE and TM waves, respectively.

The paper is organized as follows. In Section 2, we start with a brief review of existing GO representations for the transmitted fields obtained when a plane wave is incident upon a hyperbolic lens and refracted ray hits the uniaxial crystal with arbitrary orientation of the optical axis. The GO field fails at focal or caustic point. In Section 3, we applied the Maslov's method to overcome drawback of GO. In Section 4, we derived our expressions with Huygens Kirchhoff integral. In Section 5, numerical results for the 2D electromagnetic fields inside a uniaxial crystal with arbitrary orientation of the optical axis in the plane of incidence is presented. we also discuss the effects of aberrations due to an imperfect alignment of the lens and comparisons between Maslov's method and Huygens Kirchhoff integral. Finally conclusion is given in Section 6.

## 2. DERIVATION OF THE GO FIELD

Consider the geometry as shown in Figure 1. It contains a hyperbolic focusing lens placed apart from a uniaxial crystal interface. Front face of hyperbolic lens is placed at  $z = -d$  while rear face is placed at  $z = -\zeta$ . Uniaxial crystal occupies half space  $z \geq 0$ . Electromagnetic plane wave polarized in  $x$ -direction and propagating in  $z$ -direction,

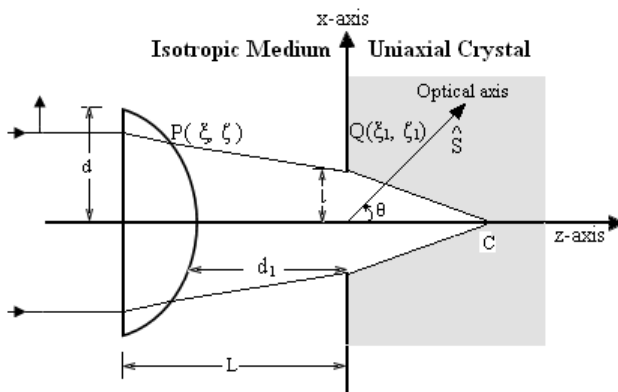


**Figure 1.** Geometry for focusing of lens into uniaxial crystal.

is incident on a hyperbolic focusing lens. After passing through the hyperbolic focusing lens, ray is refracted through plane interface of uniaxial crystal. It is assumed that uniaxial crystal occupying the half space  $z \geq 0$  has principle permittivities  $(\epsilon^o, \epsilon^e)$ , permeability  $\mu_2$ . Half space  $z < 0$  has constitutive parameters  $(\epsilon_1, \mu_1)$ . Geometry contains a hyperbolic focusing lens and is described by the following equation

$$g(\xi) = \zeta = a \left[ \frac{\xi^2}{b^2} + 1 \right]^{1/2} \quad (1)$$

where  $(\xi, \zeta)$  are the Cartesian coordinates on the lens. A linearly polarized plane wave is incident normally on the surface of the hyperbolic lens. It is assumed that the polarization of the incident wave is in  $x$  direction.

Incident plane wave is given by

$$E_x^i = \exp(-jkz) \quad (2)$$

The wave vector of the wave refracted by the cylindrical hyperbolic focusing lens is given by [23]

$$\mathbf{P} = K(\alpha) \sin \alpha \mathbf{i}_x + (n + K(\alpha) \cos \alpha) \mathbf{i}_z = p_x \mathbf{i}_x + p_z \mathbf{i}_z$$

where

$$K(\alpha) = \sqrt{1 - n^2 \sin^2 \alpha} - n \cos \alpha \quad (3)$$

Wave refracted by the hyperbolic lens hits uniaxial crystal interface. The electromagnetic field that is incident on the plane interface is TM field. The refracted field is expressed as a superposition of monochromatic ordinary and extraordinary plane waves propagating in various directions [3, 4]. Ordinary wave may be consider as TE and extraordinary wave as TM. There is no coupling between TE and TM waves. Wave vector of the refracted wave into uniaxial crystal may be obtained as [4]

$$\mathbf{p}^{et} = p_x \mathbf{i}_x + p_z^e \mathbf{i}_z \quad (4)$$

where  $z$  component may be written as

$$\begin{aligned} p_z^e &= A + \sqrt{B} \\ A &= -\frac{\chi p_x \sin \theta \cos \theta}{1 + \chi \cos^2 \theta} \\ B &= \frac{(p^o)^2(1 + \chi) - (p_x)^2}{1 + \chi \cos^2 \theta} - \frac{A^2}{\chi \cos^2 \theta} \end{aligned}$$

where  $\chi$  is measure of anisotropy in the uniaxial crystal and is given by

$$\chi = \frac{(p^e)^2}{(p^o)^2} - 1$$

$$p^e = \frac{\omega}{c} \sqrt{\epsilon^e \mu_2}$$

$$p^o = \frac{\omega}{c} \sqrt{\epsilon^o \mu_2}$$

In Equation (3), superscript  $e$  means extra-ordinary transmitted. Angle  $\theta$  is the angle of optical axis with the  $z$ -axis.

The Cartesian coordinates of the ray at front surface of the uniaxial crystal are given by

$$\xi_1 = \xi + p_x \tau_1, \quad \zeta_1 = \zeta + p_z \tau_1 \quad (5)$$

where  $\tau_1 = \frac{\zeta_1 - \zeta}{p_z}$  is distance between the point  $P(\xi, \zeta)$  on the rear face of hyperbolic lens and the point  $Q(\xi_1, \zeta_1)$  on front face of uniaxial crystal. The Cartesian coordinates of the ray refracted into the uniaxial crystal are given by

$$x = \xi_1 + p_x \tau = \xi + p_x \tau_1 + p_x \tau$$

$$z = \zeta_1 + p_z^e \tau = \zeta + p_z \tau_1 + p_z^e \tau \quad (6)$$

where  $\tau$  signifies the arc length of the ray after refraction through the uniaxial crystal. The GO solution is given by and the geometrical optics expression of field associated with the ray is given by

$$\mathbf{E}(\mathbf{r}) = \mathbf{A}_0(\xi) \left[ \frac{D(\tau)}{D(0)} \right]^{-\frac{1}{2}} \exp \left\{ -jk \left[ nS_0 + \tau_1 + \tau + \phi_0 \right] \right\} \quad (7)$$

where  $\mathbf{A}_0(\xi)$  is the amplitude of the wave at the refracted point  $(\xi, \zeta)$ . The value  $S_0$  represents the initial value of the phase function and  $\phi_0$  is a real aberration function representing possible aberrations introduced by the cylindrical lens.  $J(\tau)$  is the Jacobian of the transformation from the Cartesian to the ray coordinates, and it is given by

$$J(\tau) = \frac{D(\tau)}{D(0)} = \frac{\partial x}{\partial \xi} \frac{\partial z}{\partial \tau} - \frac{\partial z}{\partial \xi} \frac{\partial x}{\partial \tau} = \Xi + \left( \frac{\partial p_x}{\partial \xi} p_z^e - \frac{\partial p_z^e}{\partial \xi} p_x \right) \tau \quad (8)$$

where

$$\Xi = p_z^e - p_x \tan \alpha + \left( \frac{\partial p_x}{\partial \xi} p_z^e - \frac{\partial p_z^e}{\partial \xi} p_x \right) \tau_1$$

$$\frac{\partial p_x}{\partial \xi} = \frac{\partial p_x}{\partial \alpha} \frac{\partial \alpha}{\partial \xi} = DP$$

$$D = \frac{(1 - 2n^2 \sin^2 \alpha) \cos \alpha}{\sqrt{1 - n^2 \sin^2 \alpha}} - n \cos 2\alpha$$

$$P = \frac{(a^2 \cos^2 \alpha - b^2 \sin^2 \alpha)^{\frac{3}{2}}}{ab \cos \alpha}$$

It is seen that the refracted GO field fails at the singular point  $D(\tau) = 0$ . At the point satisfying (7), the ray becomes infinity.

### 3. MASLOV'S METHOD

According to the Maslov's method, the ray expression covering the caustics can be derived from the formula

$$\mathbf{E}(\mathbf{r}) = \sqrt{\frac{k}{j2\pi}} \int_{-\infty}^{\infty} \mathbf{A}_0(\xi) \left[ \frac{D(\tau)}{D(0)} \frac{\partial p_x}{\partial x} \right]^{-\frac{1}{2}} \exp \left\{ -jk \left[ nS_0 + \phi_0 + \tau_1 + \tau - p_x x(p_x, z) + p_x x \right] \right\} dp_x \quad (9)$$

In above Equation (8),  $x(p_x, z)$  means that the coordinate  $x$  should be expressed in terms of mixed coordinates  $(p_x, z)$  by using the solution. The same is true for  $\tau$  and it is given by  $\tau = \frac{z - \zeta}{p_z}$ . In the above equation  $\mathbf{A}_0(\xi)$  is an initial value of the excitation at the surface. The integrand and the phase factor are evaluated as follow

$$J(\tau) \frac{\partial p_x}{\partial x} = \frac{1}{D(0)} \frac{\partial(p_x, z)}{\partial(\xi, \tau)} = \frac{1}{D(0)} \frac{\partial p_x}{\partial \xi} \frac{\partial z}{\partial \tau} \quad (10)$$

and

$$\begin{aligned} \phi(p_x, z) &= nS_0 + \phi_0 + \tau_1 + \tau - p_x x(p_x, z) + p_x x \\ &= nS_0 + \phi_0 + \tau_1 + \tau - p_x (\xi_1 + p_x \tau) + p_x x \\ &= nS_0 + \phi_0 + \tau_1 + \tau - p_x (\xi + p_x \tau_1 + p_x \tau) + p_x x \\ &= nS_0 + \phi_0 + \tau_1 + (p_z^e)^2 \tau - p_x \xi_1 - p_x^2 \tau_1 + p_x x \\ &= nS_0 + \phi_0 + \tau_1 p_z^2 + p_x (x - \xi) + p_z^e (z - \zeta_1) \\ &= nS_0 + \phi_0 + (\zeta_1 - \zeta) p_z + K(\alpha) \sin \alpha (\rho \sin \phi - \xi) + p_z^e (z - \zeta_1) \end{aligned} \quad (11)$$

Introducing the polar coordinates

$$\begin{aligned} x &= \rho \sin \theta \\ z &= \rho \cos \theta \\ \xi &= \frac{b^2 \sin \alpha}{\sqrt{a^2 \cos^2 \alpha - b^2 \sin^2 \alpha}} \\ \zeta &= \frac{a^2 \cos \alpha}{\sqrt{a^2 \cos^2 \alpha - b^2 \sin^2 \alpha}} \end{aligned}$$

$dp_x$  is given by

$$dp_x = D d\alpha \quad (12)$$

The initial value for each component of the incident plane wave at the rear face of the lens is given by [24] as

$$\begin{aligned} \mathbf{E}_T &= \left( n \sin^2 \alpha + \sqrt{1 - n^2 \sin^2 \alpha} \right) T \mathbf{i}_x \\ &\quad + \left( n \cos \alpha - \sqrt{1 - n^2 \sin^2 \alpha} \right) T \sin \alpha \mathbf{i}_z. \end{aligned} \quad (13)$$

where

$$T = \frac{2n \cos \alpha}{\cos \alpha + n\sqrt{1 - n^2 \sin^2 \alpha}}$$

The transmission coefficients at interface of uniaxial crystal may be obtained [3] by

$$T_{\alpha}^{ee} = \frac{2\mu p^2 p_x p_z}{\mu_1(p^o)^2 p_z A^{et} - \mu p^2 B^{et}} \quad (14)$$

where

$$\begin{aligned} A^{et} &= \cos \theta p_x - \sin \theta p_z^e \\ B^{et} &= \sin \theta (p^o)^2 - p_x (\sin \theta p_x + p_z^e \cos \theta) \end{aligned}$$

Substituting (9) to (13) into (8), following results in components form is obtained as

$$\begin{aligned} E_x &= \sqrt{\frac{k}{j2\pi}} \int_{-\frac{T}{2}}^{\frac{T}{2}} E_{x0} T_{\alpha}^{ee} \left[ \frac{\Xi D}{P p_z^e} \right]^{\frac{1}{2}} \exp \{-jk[nS_0 + \phi_0 + (\zeta_1 - \zeta)p_z \\ &\quad + K(\alpha) \sin \alpha (\rho \sin \phi - \xi) + p_z^e(z - \zeta_1)]\} d\alpha \end{aligned} \quad (15)$$

$$\begin{aligned} E_z &= \sqrt{\frac{k}{j2\pi}} \int_{-\frac{T}{2}}^{\frac{T}{2}} E_{z0} T_{\alpha}^{ee} \left[ \frac{\Xi D}{P p_z^e} \right]^{\frac{1}{2}} \exp \{-jk[nS_0 + \phi_0 + (\zeta_1 - \zeta)p_z \\ &\quad + K(\alpha) \sin \alpha (\rho \sin \phi - \xi) + p_z^e(z - \zeta_1)]\} d\alpha \end{aligned} \quad (16)$$

The subtention angle  $T$  of lens is given by

$$T = \arctan \left( \frac{-ad}{b\sqrt{b^2 + d^2}} \right)$$

where  $d$  is height of hyperbolic lens.

#### 4. COMPARISON TO THE HUYGENS-KIRCHHOFF'S PRINCIPAL

To verify the validity of the uniform expression which is also valid near the caustic, we compare the numerical results with those computed from the Kirchhoff's approximation. The expression based on the Huygens-Kirchhoff principle is obtained by using Green's theorem, we can show that the refracted wave by a hyperbolic lens may be derived as

$$\mathbf{E}^r(\mathbf{r}) = \frac{1}{j4} \int_C \mathbf{A}_0(\xi) \frac{\partial E}{\partial n} H_0^{(2)}(k\tau) dl \quad (17)$$

where  $\tau = \sqrt{(x - \xi_1)^2 + (z - \zeta_1)^2} = \tau_1 p_z^2 + p_x(x - \xi_1) + p_z^e(z - \zeta_1)$  and  $\frac{\partial E}{\partial n}$  can be calculated as

$$\begin{aligned}\frac{\partial E}{\partial n} &= \frac{\partial E}{\partial x} n_x + \frac{\partial E}{\partial z} n_z = -j\omega\mu(\mathbf{N} \times \mathbf{H})_y = -j\omega\mu J_y \\ J_y &= (2\mathbf{N} \times \mathbf{H}^i)_y = -j2\omega\mu \cos\alpha \exp\left[-jk(nS_0)\right]\end{aligned}\quad (18)$$

$C$  is the contour of the lens. Using the following fact

$$dl = \sqrt{d\xi^2 + d\zeta^2} = -\frac{\sec\alpha}{P} d\alpha \quad (19)$$

and the asymptotic expression for Hankel function

$$H_0^{(2)}(k\tau) \simeq \sqrt{\frac{2}{\pi k t}} \exp[-jkt + j\pi/4] \quad (20)$$

finally the expression which is valid around the caustic is

$$E_x = -\sqrt{\frac{2}{\pi k}} \int_{-\frac{T}{2}}^{\frac{T}{2}} \frac{T_\alpha^{ee} T_{||}}{P\sqrt{\tau}} \exp[-jk(nS_0 + \tau + \phi_0 + j\pi/4)] d\alpha \quad (21)$$

$$E_z = -\sqrt{\frac{2}{\pi k}} \int_{-\frac{T}{2}}^{\frac{T}{2}} \frac{T_\alpha^{ee} T_{||}}{P\sqrt{\tau}} \exp[-jk(nS_0 + \tau + \phi_0 + j\pi/4)] d\alpha \quad (22)$$

## 5. NUMERICAL RESULT AND DISCUSSION

Field pattern around the caustic region of a hyperbolic focusing lens are obtained by performing the integration, in equations

$$\begin{aligned}E_x &= \sqrt{\frac{k}{j2\pi}} \int_{-\frac{T}{2}}^{\frac{T}{2}} E_{x0} T_\alpha^{ee} \left[ \frac{\Xi D}{P p_z^e} \right]^{\frac{1}{2}} \\ &\exp\{-jk[nS_0 + \phi_0 + (\zeta_1 - \zeta)p_z + K(\alpha) \sin\alpha(\rho \sin\phi - \xi) + p_z^e(z - \zeta_1)]\} d\alpha\end{aligned}$$

and

$$E_x = -\sqrt{\frac{2}{\pi k}} \int_{-\frac{T}{2}}^{\frac{T}{2}} \frac{T_\alpha^{ee} T_{||}}{P\sqrt{\tau}} \exp[-jk(nS_0 + \tau + \phi_0 + j\pi/4)] d\alpha$$

numerically by using Mathcad software. Throughout the discussion, we have used refractive index of hyperbolic lens  $n = 2.8$ . Figure 2 provides comparison between Maslov's method and Kirchhoff's approximation. The solid line shows the results obtained using Maslov's method while dashed line is for result obtained using Huygens-Kirchhoff's Principal which are in good agreement. Both the curves behaves similarly ; for example, we have the same number of peaks for each curve, situated at

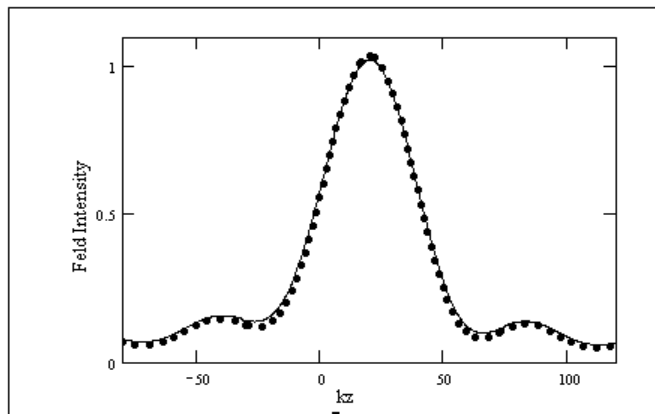


**Figure 2.** Comparison of normalized intensity at caustic point using Maslovs method (dotted line) and  $K$ - $H$  integral (solid line) at  $\theta_0 = 0$ .

about the same position. Maslov's method takes advantage of the fact that the occurrence of caustics is formulation dependent and corrects all types of caustics by combining the simplicity of ray theory and generality of the transform method. It is actually easy to implement and is faster to compute the data than other methods.

Figure 3 to Figure 7 show comparison of field distribution at different orientation of optical axis that is at  $\theta = 0^\circ$ ,  $\theta = 30^\circ$ ,  $\theta = 45^\circ$ ,  $\theta = 60^\circ$ ,  $\theta = 75^\circ$  and  $\theta = 90^\circ$ . Figure 8 to Figure 10 show contour plots of field distribution at different orientation of optical axis that is at  $\theta = 0^\circ$ ,  $\theta = 45^\circ$  and  $\theta = 90^\circ$ . It is observed that the focal region for a negative uniaxial crystal is displaced in the  $x$  and  $z$  directions as the angle  $\theta$  is increased from  $\theta = 0^\circ$ . If we continue to increase the angle  $\theta$ , we will obtain a maximum displacement of the focal area when  $\theta = 45^\circ$ . If the angle  $\theta$  is increased above  $\theta = 45^\circ$ , then the displacement of the focal area will be reduced until  $\theta$  approaches  $\theta = 90^\circ$ . The results displayed in Figure 6 show that the maximum intensities are indeed the same, as expected, but the focus in the crystal is shifted towards the interface compared to the focus in the isotropic medium. The crystal can be replaced by an isotropic medium by putting  $n^e = n^o = 2$ . Throughout the discussion, for uniaxial crystal case, we have used LiNbO<sub>3</sub>, which has ordinary refractive index of  $n^o = 2.3$  and an extraordinary refractive index of  $n^e = 2.208$ . It is assumed that  $ka = 14$ ,  $kb = 13$ ,  $kd = 14$ . The distance between the rear face of the lens and front face of uniaxial crystal  $kd_1 = 5$ . The realization of parameter of scheme may be observed from Figure 7 as

maximum field intensity is at  $kc = 19.1$  by using  $c = \sqrt{a^2 + b^2}$ . All these parameter are normalized by wavelength  $\lambda$ .

It is difficult to construct an aberration free system, so it is important for us to include effect of possible aberration for any

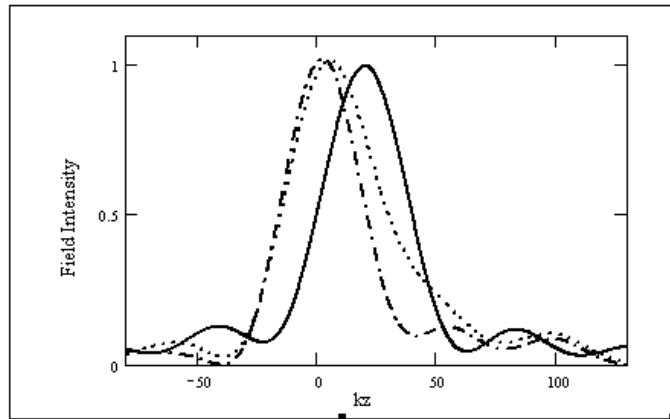


**Figure 3.** Normalized field Intensity distribution around caustic point along  $z$ -axis at  $\theta = 0^\circ$  (solid line),  $\theta = 30^\circ$  (dotted line) and  $\theta = 45^\circ$  (dashed line) at  $ka = 14$ ,  $kb = 13$  and  $kd = 14$ .

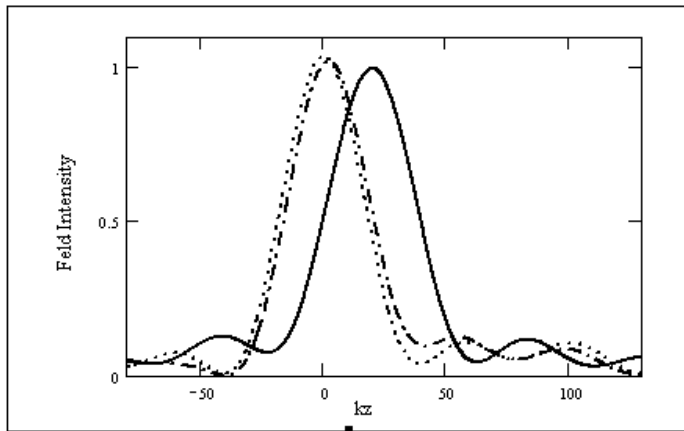


**Figure 4.** Normalized field Intensity distribution around caustic point along  $z$ -axis at  $\theta = 0^\circ$  (solid line),  $\theta = 45^\circ$  (dotted line) and  $\theta = 60^\circ$  (dashed line)  $ka = 14$ ,  $kb = 13$  and  $kd = 14$ .

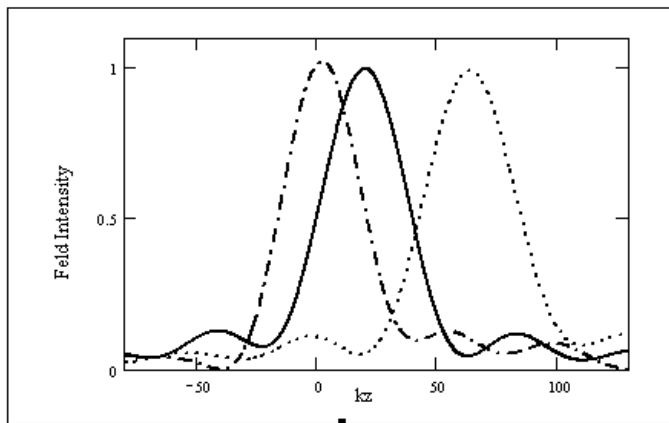


**Figure 5.** Normalized field Intensity distribution around caustic point along  $z$ -axis at  $\theta = 0^\circ$  (solid line),  $\theta = 45^\circ$  (dashed line) and  $\theta = 90^\circ$  (dotted line) at  $ka = 14$ ,  $kb = 13$  and  $kd = 14$ .

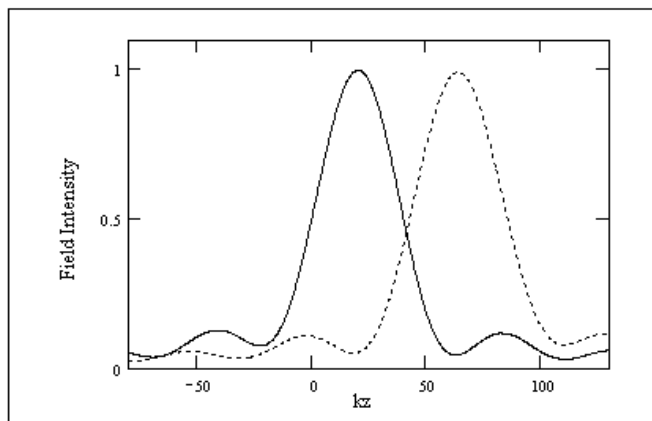


**Figure 6.** Comparison of normalized field intensity distribution around the caustic region with optical axis in pointing in  $x$  direction at  $\theta = 90^\circ$  (dotted line) and  $z$  direction at  $\theta = 0^\circ$  (solid line).

focussing antenna. In presence of aberration there is no astigmatism, and the field curvature is quadratic in  $\xi_1$  and can cause focal shift. In this case aberrations are of two types will be of our interest when studying the distribution of the intensity in the caustic region. These aberrations are known as cylindrical aberration and coma aberration. The aberration symbol  $\phi_0$  in above Equation (6) can be represented [5]

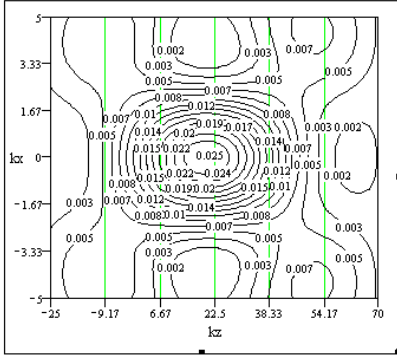


**Figure 7.** Contour plot of focused field intensity distribution around the caustic region at  $\theta = 0^\circ$ ,  $ka = 14$ ,  $kb = 13$  and  $kd = 14$ .

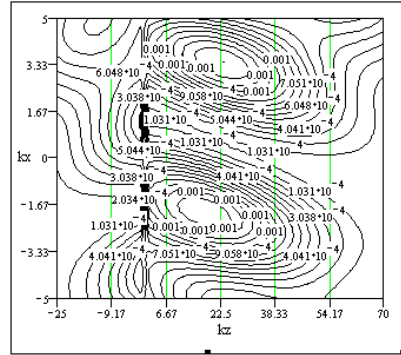


**Figure 8.** Contour plot of normalized field intensity distribution around the caustic region at  $\theta = 45^\circ$ ,  $ka = 10$ ,  $kb = 14$  and  $kd = 15$ .

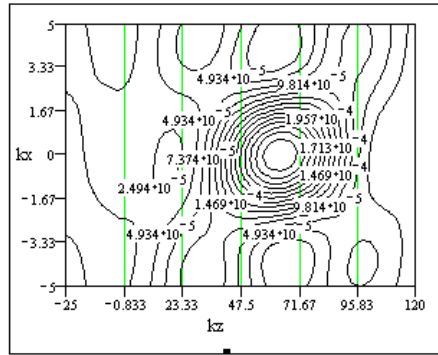


**Figure 9.** Contour plot of field intensity distribution around the caustic region at  $\theta = 90^\circ$ ,  $ka = 14$ ,  $kb = 13$  and  $kd = 14$ .

by

$$\phi_0 = -\delta_1 \lambda_1 \left( \frac{\xi_1}{l} \right)^4 + \delta_2 \lambda_1 \left( \frac{\xi_1}{l} \right)^3$$

where  $l$  is the half width of the slit aperture of crystal. The first term in above equation represents the cylindrical aberration and the second one the coma aberration. The symbol  $\delta_1$  and  $\delta_2$  are the wave-front deformations at the edge of the slit aperture measured in units of the wavelength in the isotropic medium. The effects of cylindrical

aberration and coma were discussed in [6, 7]. According to the results a first-order cylindrical aberration causes a focal shift towards or away from the aperture plane depending on whether the aberration is positive ( $\delta_1 > 0$ ) or negative ( $\delta_1 < 0$ ). Such a phenomenon is also discussed in [7] as an aberration introduced when focusing from an optically denser medium into an optically rarer medium ( $\delta_1 > 0$ ), or from an optically rarer medium into an optically denser medium ( $\delta_1 < 0$ ).

When we consider the effect of a first order cylindrical aberration for the case in which the second medium is a negative uniaxial crystal  $\text{LiNbO}_3$ , and we examine whether the effect is different from that obtained when the second medium is isotropic. In all cases considered in this paper the refractive index of the first medium was  $n_1 = 1$ . Figure 10 shows a comparison between the field intensities distribution obtained when the second medium is either uniaxial or isotropic for the case in which the incident wave front has no aberrations. When the second medium was considered as isotropic the refractive index was  $n_2 = 2.00$ . When the second medium was considered as uniaxial crystal, we used  $\text{LiNbO}_3$ , which has an ordinary refractive index of  $n^o = 2.300$  and an extraordinary refractive index of  $n^e = 2.208$ . The interface of the second medium was placed at a distance of  $kd_1 = 5$  from the aperture plane, and the optical axis of the crystal was assumed to be in the  $xz$  plane.

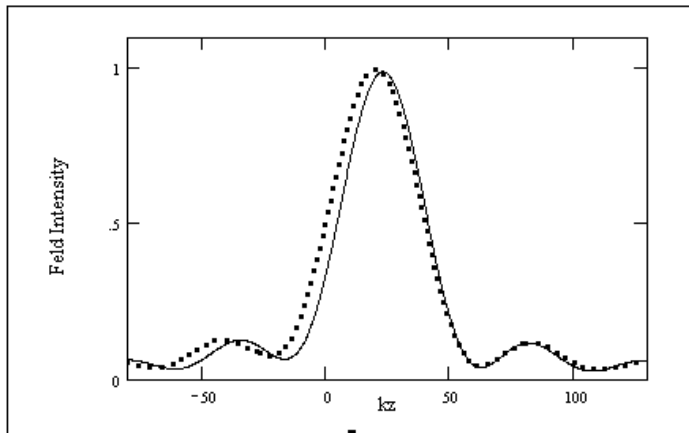


**Figure 10.** Comparsion between focused fields in an isotropic medium (solid line) and a uniaxial crystal (dashed line) in the absence of aberrations at  $\theta = 0^\circ$ ,  $ka = 14$ ,  $kb = 13$  and  $kd = 14$ .

Figure 11 shows a comparison of two focussed field intensities obtained for the case in which the second medium is isotropic. One of the line plot corresponds to the aberration-free case, while the other line plot corresponds to the case in which the incident wave

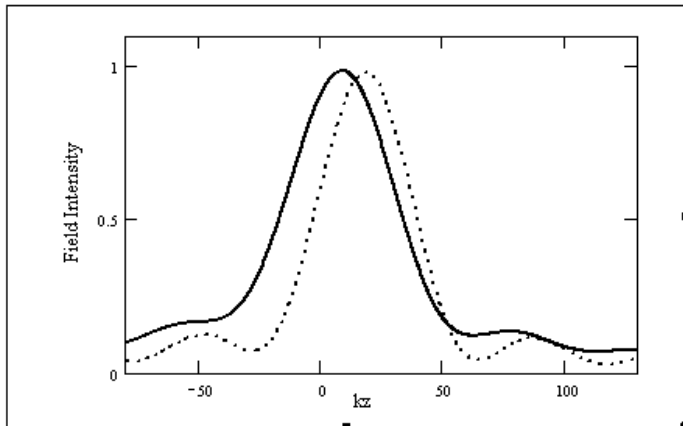


**Figure 11.** Variation of intensity in an isotropic medium without aberration (dashed line) and with aberration (solid line) of  $\delta_1 = 0.2$  at  $\theta_0 = 0$ .

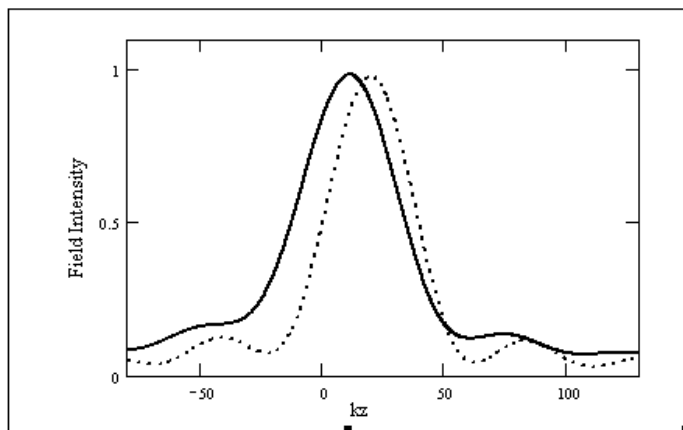
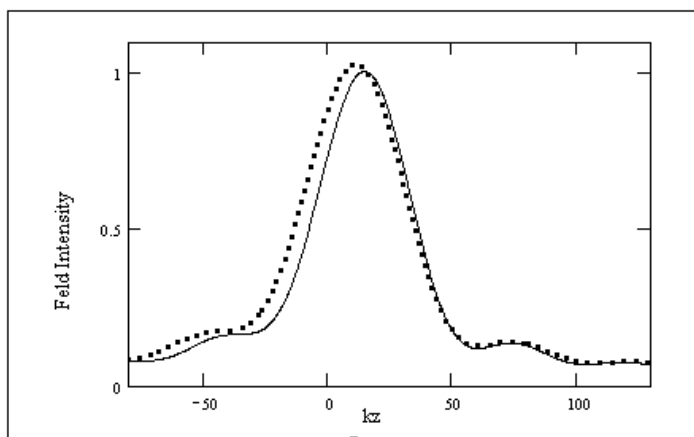


**Figure 12.** Variation of intensity in a uniaxial crystal without aberration (solid line) and with aberration (dashed line) of  $\delta_1 = 0.2$  at  $\theta_0 = 0$ .

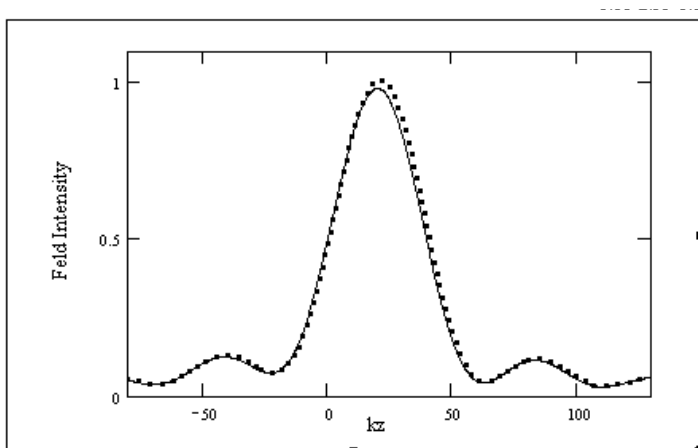
front has a positive first-order cylindrical aberration of 0.2 wavelengths  $\delta_1 = 0.2$ . Figure 12 shows a comparison of two field intensities obtained for the case in which the second medium is a uniaxial crystal, and one of the curves corresponds to aberration-free case, while the other curve corresponds to the case in which a positive first-order cylindrical aberration of 0.2 wavelengths  $\delta_1 = 0.2$  was added to the incident wave front. Figure 13 shows a comparison of two field intensities obtained when the second medium is either isotropic or uniaxial for the case in which the incident wave front has a positive first-order cylindrical aberration of 0.2 wavelengths  $\delta_1 = 0.2$ .

Figure 14 shows a comparison of two field intensities obtained for the case in which the second medium is a uniaxial crystal, and one of the curves corresponds to aberration-free case, while the other curve corresponds to the case in which a positive coma aberration of 0.05 wavelengths ( $\delta_2 = 0.052$ ) was added to the incident wave front.

From Figure 10 to Figure 14, we conclude that in the presence of aberrations the focal shift has the same behavior in the uniaxial case as in the isotropic case. Although the position of the focus is different in the two cases, the shape of the axial intensities is similar in both cases. Secondly we see from that the maximum axial intensity is increased when a positive first-order aberration is added to the incident wave front.



**Figure 13.** Variation of intensity in an isotropic medium (solid line) and uniaxial crystal (dashed line) with aberration of  $\delta_1 = 0.2$  at  $\theta_0 = 0$ .



**Figure 14.** Variation of intensity in a uniaxial crystal without aberration(solid line) and in presence of coma aberration of  $\delta_2 = 0.2$  at  $\theta_0 = 0$ .

## 6. CONCLUSIONS

Our comparisons between Maslov's method and Huygens-Kirchhoff's integral results for 2D electromagnetic waves focused from hyperbolic lens into uniaxial crystals are in good agreement. We have observed that the caustic point in a negative uniaxial crystal is toward aperture slit as compared to the caustic point obtained in the corresponding isotropic medium. When the optical axis is transverse to the interface normal that is pointing towards  $x$  direction, the caustic point is farther away from the interface than the caustic point when the optical axis is parallel to the interface normal.

We have also found that the aberration can give a focal shift towards or away from the aperture plane depending on whether the aberration is positive or negative. If a small aberration is added onto the incident wave front, the maximum axial intensity may increase, because the aberration leads to a focal shift towards the aperture plane, and because the secondary wavelets are stronger in front of the focus than behind the focus.

## REFERENCES

1. Stamnes, J. J., *Waves in Focal Regions*, Adam Hilger, Bristol, Boston, 1986.
2. Stamnes, J. J. and G. C. Sherman, "Radiation of electromagnetic

- fields in uniaxially anisotropic media," *J. Opt. Soc. Am.*, Vol. 66, No. 8, 780–788, 1976.
- 3. Stamnes, J. J. and D. Jiang, "Focusing of electromagne waves into a uniaxial crystal," *Opt. Comm.*, Vol. 150, 251–262, 1998.
  - 4. Jiang, D. and J. J. Stamnes, "Numerical and asymptotic results for focusing of two-dimensional electromagnetic waves in uniaxial crystals," *Opt. Comm.*, Vol. 163, 55–71, 1999.
  - 5. Jiang, D. and J. J. Stamnes, "Numerical and experimental results for focusing of two-dimensional electromagnetic waves into uniaxial crystals," *Opt. Comm.*, Vol. 174, 321–334, 2000.
  - 6. Stamnes, J. J. and D. Jiang, "Focusing of two-dimensional electromagnetic waves through a plane interface," *Pure Appl. Opt.*, Vol. 7, 603–625, 1998.
  - 7. Jiang, D. and J. J. Stamnes, "Focusing at low Fresnel numbers in the presence of cylindrical or spherical aberration," *Pure Appl. Opt.*, Vol. 7, 85–93, 1998.
  - 8. Yariv, A. and P. Yeh, *Optical Waves in Crystals: Propagation and Control of Laser Radiation*, 1984.
  - 9. Boyenga, D. L. and C. N. Mabika, "Rigorous analysis of uniaxial discontinuities microwave components using a new multimodal variational formulation," *Progress In Electromagnetics Research B*, Vol. 2, 61–71, 2008.
  - 10. Urbani, F., "Numerical analysis of periodic planar structures on uniaxial substrates for miniaturization purposes," *Progress In Electromagnetics Research Letters*, Vol. 5, 131–36, 2008.
  - 11. Khalilpour, J. and M. Hakkak, "S-shaped ring resonator as anisotropic uniaxial metamaterial used in waveguide tunneling," *Journal of Electromagnetic Waves and Applications*, Vol. 23, No. 13, 1763–1772, 2009.
  - 12. Zheng, K. S., W. Y. Tam, D. B. Ge, and J. D. Xu, "Uniaxial PML absorbing boundary condition for truncating the boundary of dng metamaterials," *Progress In Electromagnetics Research*, Vol. 8, 125–34, 2009.
  - 13. Luukkonen, O., C. R. Simovski, and S. A. Tretyakov, "Grounded uniaxial material slabs as magnetic conductors," *Progress In Electromagnetics Research*, Vol. 15, 267–283, 2009.
  - 14. Lv, C. J., Y. Shi, and C. H. Liang, "Higher order hierarchical legendre basis functions application to the analysis of scattering by uniaxial anisotropic objects," *Progress In Electromagnetics Research M*, Vol. 13, 133–143, 2010.
  - 15. Wolf, E., "Electromagnetic diffraction in optical systems I. An

- integral representation of the image field," *Proc. Roy. Soc. London A*, Vol. 253, 349–357, 1959.
- 16. Richards, B. and E. Wolf, "Electromagnetic diffraction in optical systems II. Structure of the image field in an aplanatic system," *Proc. Roy. Soc. London A*, Vol. 253, 358–379, 1959.
  - 17. Gong, Y. and G. Wang, "Superficial tumor hyperthermia with flat left-handed metamaterial lens," *Progress In Electromagnetics Research*, Vol. 98, 389–405, 2009.
  - 18. Hansen, R. C. (ed.), *Geometrical Theory of Diffraction*, IEEE Press, New York, NY, 1988.
  - 19. Maslov, V. P., *Perturbation Theory and Asymptotic Method*, Moskov. Gos. Univ., Moscow, 1965 (in Russian translated into Japanese by Ouchi et al., Iwanami, Tokyo, 1976).
  - 20. Gorman, A. D., "Vector field near caustics," *J. Math. Phys.*, Vol. 26, 1404–1407, 1985.
  - 21. Ziolkowski, R. W. and G. A. Deschamps, "Asymptotic evaluation of high frequency fields near a caustic, an introduction to Maslov's method," *Radio Sci.*, Vol. 19, No. 4, 1001–1025, 1984.
  - 22. Ji, Y. and K. Hongo, "Field in the focal region of a dielectric spherical lens," *J. Opt. Soc. Am. A*, Vol. 8, 1721–1728, 1991.
  - 23. Hongo, K. and H. Kobayashi, "Radiation characteristics of a plano convex lens antenna," *Radio Sci.*, Vol. 31, No. 5, 1025–1035, 1987.
  - 24. Ghaffar, A., A. Hussain, Q. A. Naqvi, and K. Hongo, "Radiation characteristics of an inhomogeneous slab," *Journal of Electromagnetic Waves and Applications*, Vol. 22, No. 2, 301–312, 2008.
  - 25. Rahim, T. and M. J. Mughal, "Spherical reflector in chiral medium supporting positive phase velocity and negative phase velocity simultaneously," *Journal of Electromagnetic Waves and Applications*, Vol. 23, 1665–1673, 2009.
  - 26. Mehmood, M. Q., M. J. Mughal, and T. Rahim, "Focal region fields of cassegrain system placed in homogeneous chiral medium," *Progress In Electromagnetics Research B*, Vol. 21, 329–346, 2010.
  - 27. Mehmood, M. Q., M. J. Mughal, and T. Rahim, "Focal region fields of gregorian system placed in homogeneous chiral medium," *Progress In Electromagnetics Research M*, Vol. 11, 241–256, 2010.